

Censored Graphical Horseshoe: Bayesian sparse precision matrix estimation with censored and missing data

The Tien Mai¹ and Sayantan Banerjee²

¹Norwegian Institute of Public Health, Oslo, 0456, Norway.

²OM & QT Area, Indian Institute of Management Indore, M.P. 453556, India.

Email: the.tien.mai@fhi.no,
sayantanb@iimidr.ac.in

Abstract

Gaussian graphical models provide a powerful framework for studying conditional dependencies in multivariate data, with widespread applications spanning biomedical, environmental sciences, and other data-rich scientific domains. While the Graphical Horseshoe (GHS) method has emerged as a state-of-the-art Bayesian method for sparse precision matrix estimation, existing approaches assume fully observed data and thus fail in the presence of censoring or missingness, which are pervasive in real-world studies. In this paper, we develop the Censored Graphical Horseshoe (CGHS), a novel Bayesian framework that extends the GHS to censored and arbitrarily missing Gaussian data. By introducing a latent-variable representation, CGHS accommodates incomplete observations while retaining the adaptive global-local shrinkage properties of the Horseshoe prior. We derive efficient Gibbs samplers for posterior computation and establish new theoretical results on posterior behavior under censoring and missingness, filling a gap not addressed by frequentist Lasso-based methods. Through extensive simulations, we demonstrate that CGHS consistently improves estimation accuracy compared to penalized likelihood approaches. Our methods are implemented in the package `GHScenmis` available on Github: <https://github.com/tienmt/ghscenmis>.

Keywords: Graphical models, censored data, missing data, shrinkage priors.

1 Introduction

Gaussian graphical models (GGMs) are a central tool for modeling conditional dependencies among multivariate random variables, with applications in fields ranging from genomics and neuroimaging to finance [35, 37, 15, 11]. In GGMs, the precision matrix $\Omega = \Sigma^{-1} \in \mathbb{R}^{p \times p}$ encodes the conditional independence structure: a zero in an off-diagonal entry indicates conditional independence between the corresponding nodes [20]. Estimating sparse precision matrices is particularly important in high-dimensional settings, where the number of variables p may be comparable to or larger than the sample size n , and sparsity can be leveraged to recover the underlying graph structure. Popular frequentist approaches include the graphical lasso [16], graphical SCAD [14], and CLIME [9], which provide consistent estimators of high-dimensional inverse covariance matrices under various sparsity patterns [10, 19].

Bayesian methods for precision matrix estimation offer adaptive regularization and uncertainty quantification, but work in this area is relatively limited. [41] proposed a Bayesian graphical lasso via block Gibbs sampling, while [6] introduced a prior combining a continuous shrinkage component with a point-mass at zero for off-diagonal entries, deriving posterior contraction rates and Laplace approximations for model selection. Spike-and-slab variants with double-exponential priors were explored by [17], and [2] used a quasi-likelihood approach with favorable posterior contraction. A limitation of spike-and-slab priors is the presence of binary indicators, which can impede posterior exploration.

The Graphical Horseshoe (GHS) prior [21] overcomes this challenge by applying global-local shrinkage to precision matrices, providing strong adaptive regularization and superior empirical performance compared to both frequentist and Bayesian alternatives. Recent work has further explored variants of the Horseshoe prior, including pseudo-likelihood approaches [42] and Horseshoe-like priors [38].

In practice, data often include censored or missing values, particularly in biomedical, environmental, or epidemiological studies where measurements may fall below detection limits, see for example [13, 31, 36, 34]. Ignoring censoring or missingness can lead to biased inference, yet methods to handle such data within high-dimensional Bayesian GGMs remain scarce. Early work on covariance estimation with missing or censored data was developed by [22, 33], but these methods were not Bayesian. Frequentist approaches for censored graphical lasso have been proposed in [3, 39], with software implementations available in [4], but Bayesian alternatives remain underdeveloped.

In this paper, we extend the Graphical Horseshoe to handle censored and arbitrarily missing Gaussian data. Our censored Graphical Horseshoe (CGHS) model introduces a latent-variable formulation to account for censored observations and missingness, while leveraging the adaptive shrinkage properties of the Horseshoe prior to recover sparse precision matrices. This approach allows robust inference of conditional dependencies in challenging real-world datasets where standard GHS methods may fail.

To perform posterior inference for our model, we have developed a Gibbs sampler that updates a block of parameters and latent variables in each step. The sampler cycles through several key steps: first, it imputes censored latent values or imputes the missing data; second, it updates the regression parameters and residual variances; third, it adapts the local and global shrinkage scales; and finally, it reconstructs the precision matrix. This process generates samples from the joint posterior distribution of the model parameters and latent variables, which can then be used to form reliable estimates of the underlying graphical structure.

We also develop a comprehensive set of theoretical results that characterize the behavior of the posterior distribution in each of the settings we consider. This aspect of our work is genuinely novel, and to the best of our knowledge, no theoretical result has been established for the frequentist methods in complex scenarios involving censoring or missingness. More specifically, we derive posterior concentration rates of the precision matrix for both censored-data and missing-data regimes. These results provide rigorous justification for the stability and reliability of our Bayesian formulation, demonstrating that the method adapts to the underlying signal even under challenging data-generating mechanisms.

In addition to our theoretical contributions, we present an extensive suite of simulation studies designed to assess the finite-sample performance of the proposed approach. Across a broad range of sparsity levels, noise structures, and censoring or missing-data patterns, our Bayesian estimator frequently outperforms its Lasso-based counterparts. Finally, we illustrate the practical utility of our method through an application to single-cell data, where the model successfully captures key biological signals while accommodating the intrinsic sparsity and uncertainty in these datasets.

The rest of the paper is presented as follows. Section 2 present models and our approach with Gibbs sampler for the case of censored data. Section 3 present models and our approach with Gibbs sampler for the case of missing data. Numerical studies with simulations and a real data application are given in Section 4 and Section 5. Theoretical results are presented in Section 6 with proofs in Appendix B. We discuss and conclude in Section 7. Additional simulation results and plots are in Appendix A.

2 Censored graphical Horseshoe

2.1 Model specification

Let $Y = (Y_1, \dots, Y_n) \in \mathbb{R}^{n \times p}$ denote the data matrix, where each $Y_i \sim \mathcal{N}_p(0, \Omega^{-1})$. Here Ω denotes the precision (inverse-covariance) matrix. In practice, however, the variables are not always fully observed; instead, the measurements are subject to left censoring at variable-specific thresholds. For each coordinate j , if the true value Y_{ij} falls below a censoring threshold c_j , we only record the threshold itself. Thus, the

observed values take the form

$$\tilde{Y}_{ij} = \begin{cases} Y_{ij}, & \text{if } Y_{ij} > c_j, \\ c_j, & \text{if } Y_{ij} \leq c_j, \end{cases} \quad (1)$$

for $i \in \{1, \dots, n\}$ and $j \in \{1, \dots, p\}$.

To deal with censoring, we introduce latent uncensored variables $Z = (Z_1, \dots, Z_n)^\top \in \mathbb{R}^{n \times p}$ with the same distribution as the original Gaussian model, that is, $Z_i \sim \mathcal{N}_p(0, \Omega^{-1})$. The observed data are then related to the latent process through $\tilde{Y}_{ij} = \max(Z_{ij}, c_j)$. Inference therefore focuses on the sparse precision matrix Ω given the censored observations \tilde{Y} .

For each observation i , we define the sets

$$\mathcal{O}_i = \{j : \tilde{Y}_{ij} > c_j\}, \quad \text{and} \quad \mathcal{C}_i = \{j : \tilde{Y}_{ij} = c_j\}$$

to denote the indices of uncensored and censored entries, respectively. Partitioning Z_i accordingly, the observed data likelihood can be expressed as a product of Gaussian density terms for the uncensored components and multivariate Gaussian distribution function terms for the censored ones:

$$L(\Omega; \tilde{Y}) = \prod_{i=1}^n \phi_{|\mathcal{O}_i|}(\tilde{Y}_{i,\mathcal{O}_i}; 0, \Sigma_{\mathcal{O}_i, \mathcal{O}_i}) \cdot \Phi_{|\mathcal{C}_i|}(c_{\mathcal{C}_i} \mid \mu_{i,\mathcal{C}_i|\mathcal{O}_i}, \Sigma_{\mathcal{C}_i|\mathcal{O}_i}), \quad (2)$$

where $\Sigma = \Omega^{-1}$, and the conditional mean and covariance of the censored components given the observed ones are

$$\begin{aligned} \mu_{i,\mathcal{C}_i|\mathcal{O}_i} &= \Sigma_{\mathcal{C}_i, \mathcal{O}_i} \Sigma_{\mathcal{O}_i, \mathcal{O}_i}^{-1} \tilde{Y}_{i,\mathcal{O}_i}, \\ \Sigma_{\mathcal{C}_i|\mathcal{O}_i} &= \Sigma_{\mathcal{C}_i, \mathcal{C}_i} - \Sigma_{\mathcal{C}_i, \mathcal{O}_i} \Sigma_{\mathcal{O}_i, \mathcal{O}_i}^{-1} \Sigma_{\mathcal{O}_i, \mathcal{C}_i}. \end{aligned}$$

2.2 Prior specification

To induce sparsity in the precision matrix, as in [21], we place the graphical Horseshoe prior on the off-diagonal entries. For indices $j < k$, the prior specification takes the hierarchical form

$$\begin{aligned} \omega_{jk} \mid \lambda_{jk}, \tau &\sim \mathcal{N}(0, \lambda_{jk}^2 \tau^2), \\ \lambda_{jk} &\sim \mathcal{C}^+(0, 1), \\ \tau &\sim \mathcal{C}^+(0, 1), \end{aligned} \quad (3)$$

where \mathcal{C}^+ denotes the half-Cauchy distribution. The diagonal elements ω_{jj} are constrained to ensure positive definiteness and are typically assigned noninformative priors or estimated under such constraints.

Each coefficient is assigned its own scale factor, denoted by λ_{jk} , which acts as a local shrinkage parameter, while a common scale factor, τ , serves as the global shrinkage parameter across all coefficients. This hierarchical prior structure produces two desirable effects: a sharp concentration of prior mass around zero, which aggressively suppresses noise variables, and heavy tails, which allow large, informative signals to remain largely unaffected [12].

2.3 Data augmentation for censoring

The censored structure naturally lends itself to a data augmentation approach in which the latent Gaussian variables Z are treated as missing data. Given observations data \tilde{Y} and the censoring thresholds (c_1, \dots, c_p) , the augmented variables Z_{ij} are updated from their conditional distributions. If an observation is uncensored, then Z_{ij} coincides with \tilde{Y}_{ij} and follows its conditional Gaussian law. If an observation is censored, then Z_{ij} is drawn from the same Gaussian distribution but truncated to the region $(-\infty, c_j]$. Formally, the conditional distribution takes the form

$$Z_{ij} \mid \tilde{Y}_{ij}, \Omega, Z_{i,-j} \sim \begin{cases} \mathcal{N}(\mu_{ij}, \sigma_j^2), & \text{if } \tilde{Y}_{ij} = Z_{ij}, \\ \mathcal{N}(\mu_{ij}, \sigma_j^2) \mathbb{I}(Z_{ij} \leq c_j), & \text{if } \tilde{Y}_{ij} = c_j, \end{cases}$$

where μ_{ij} and σ_j^2 are derived from the conditional distribution of Z_{ij} given the remaining coordinates under the multivariate normal model:

$$Z_{ij} \mid Z_{i,-j} \sim \mathcal{N} \left(-\frac{1}{\omega_{jj}} \sum_{k \neq j} \omega_{jk} Z_{ik}, \omega_{jj}^{-1} \right).$$

2.4 Gibbs sampler for censored Graphical Horseshoe

2.4.1 Parameterization via nodewise regression

To parameterize Ω , we adopt the nodewise regression framework [32, 40]. Denoting $Z_{\cdot j}$ as the j th column of Z , and $Z_{\cdot,-j}$ the $n \times (p-1)$ submatrix of Z excluding column j , the conditional distribution of $Z_{\cdot j}$ given the remaining variables is modeled as

$$Z_{\cdot j} \mid Z_{\cdot,-j}, \theta_j, \sigma_j^2 \sim \mathcal{N}(Z_{\cdot,-j} \theta_j, \sigma_j^2 I_n), \quad j = 1, \dots, p,$$

where $\theta_j \in \mathbb{R}^{p-1}$ collects the regression coefficients and $\sigma_j^2 > 0$ is the conditional variance. The connection to the precision matrix is explicit:

$$\Omega_{jj} = \sigma_j^{-2}, \quad \Omega_{-j,j} = -\sigma_j^{-2} \theta_j.$$

Since each of the p regressions yields a separate estimate, a symmetrization step (described below) is necessary to reconcile them into a single symmetric precision matrix. In this form, we have that, for each coefficient θ_{jk} with $k \neq j$,

$$\theta_{jk} \mid \lambda_{jk}^2, \tau_j^2, \sigma_j^2 \sim \mathcal{N}(0, \sigma_j^2 \tau_j^2 \lambda_{jk}^2),$$

with local shrinkage λ_{jk}^2 and global shrinkage τ_j^2 . Following Carvalho et al. [12], the prior hierarchy is

$$\begin{aligned} \lambda_{jk}^2 \mid \nu_{jk} &\sim \text{Inv-Gamma}(1, \nu_{jk}^{-1}), & \nu_{jk} &\sim \text{Inv-Gamma}(1, 1), \\ \tau_j^2 \mid \xi_j &\sim \text{Inv-Gamma}\left(\frac{m+1}{2}, \xi_j^{-1}\right), & \xi_j &\sim \text{Inv-Gamma}(1, 1), \end{aligned}$$

where $m = p - 1$. The residual variance is assigned an inverse-gamma prior, $\sigma_j^2 \sim \text{Inv-Gamma}(a_0, b_0)$. Note that, here we use the shape–rate parameterization, with density of $\text{Inv-Gamma}(a, b)$ proportional to $x^{-a-1} \exp(-b/x)$.

Conditional on (θ_j, σ_j^2) , the latent Z_{ij} has conditional mean $\mu_{ij} = z_{i,-j}^\top \theta_j$ and variance σ_j^2 . The observation mechanism is defined as

- (a) If $Y_{ij} > c_j$ (uncensored), then $Z_{ij} = Y_{ij}$ is fully observed.
- (b) If $Y_{ij} = c_j$ (censored), then Z_{ij} follows a truncated normal distribution,

$$Z_{ij} \mid \mathcal{C}_{ij} = 1 \sim \mathcal{N}(\mu_{ij}, \sigma_j^2) \text{ with support } (-\infty, c_j].$$

2.4.2 Posterior computation

Posterior inference is carried out by means of a Gibbs sampler in which each block of parameters and latent variables is updated in turn. The sampler alternates between imputing censored latent values, updating regression parameters, adapting local and global shrinkage scales, and reconstructing the precision matrix. We now describe each component of the algorithm in detail.

The first step of the sampler updates the latent Gaussian data Z . When an observation is uncensored, so that $Y_{ij} > c_j$, the corresponding latent value is deterministically set to $Z_{ij} = Y_{ij}$. For censored

observations with $Y_{ij} = c_j$, the latent entry is drawn from a truncated normal distribution with mean $\mu_{ij} = z_{i,-j}^\top \theta_j$ and variance σ_j^2 , truncated above at c_j :

$$Z_{ij} \sim \mathcal{N}(\mu_{ij}, \sigma_j^2) \text{ restricted to } (-\infty, c_j]. \quad (4)$$

Given the augmented data, the regression coefficients θ_j are updated from their Gaussian full conditional. For each node $j \in \{1, \dots, p\}$, define the response vector $y_j = Z_{\cdot,j}$ and the predictor matrix $X^{(j)} = Z_{\cdot,-j}$. The conditional Gaussian likelihood yields the regression model

$$y_j = X^{(j)}\theta_j + \varepsilon_j, \quad \varepsilon_j \sim \mathcal{N}(0, \sigma_j^2 I_n).$$

The horseshoe prior is placed on the regression coefficients:

$$\theta_{jk} \mid \lambda_{jk}, \tau_j, \sigma_j^2 \sim \mathcal{N}(0, \sigma_j^2 \tau_j^2 \lambda_{jk}^2), \quad \lambda_{jk} \sim \mathcal{C}^+(0, 1), \quad \tau_j \sim \mathcal{C}^+(0, 1).$$

The posterior updates proceed as follows. The conditional covariance and mean of the regression coefficients are

$$V_j = \left(X^{(j)\top} X^{(j)} + \text{diag}\left(\frac{1}{\tau_j^2 \lambda_{jk}^2}\right) \right)^{-1}, \quad \mu_{\theta_j} = V_j X^{(j)\top} y_j,$$

and the coefficients are updated via $\theta_j \sim \mathcal{N}(\mu_{\theta_j}, \sigma_j^2 V_j)$.

The residual variance is updated from its inverse-gamma conditional posterior,

$$\sigma_j^2 \sim \text{Inv-Gamma}\left(a_0 + \frac{n}{2}, b_0 + \frac{1}{2} \|y_j - X^{(j)}\theta_j\|^2\right).$$

The local scales are updated using the Makalic–Schmidt parameterization,

$$\lambda_{jk}^2 \sim \text{Inv-Gamma}\left(1, \frac{1}{\nu_{jk}} + \frac{\theta_{jk}^2}{2\sigma_j^2 \tau_j^2}\right), \quad \nu_{jk} \sim \text{Inv-Gamma}(1, 1 + 1/\lambda_{jk}^2),$$

and the global scale parameter is updated as

$$\tau_j^2 \sim \text{Inv-Gamma}\left(\frac{m+1}{2}, \frac{1}{\xi_j} + \sum_k \frac{\theta_{jk}^2}{2\sigma_j^2 \lambda_{jk}^2}\right), \quad \xi_j \sim \text{Inv-Gamma}(1, 1 + 1/\tau_j^2).$$

Once all nodewise regressions are updated, the precision matrix Ω is reconstructed. The diagonal elements are determined by the inverse residual variances: $\Omega_{jj} = 1/\sigma_j^2$, and the off-diagonal elements are obtained from the regression coefficients: $\Omega_{-j,j} = -\theta_j/\sigma_j^2$. Because each regression is updated separately, the reconstructed matrix may not be perfectly symmetric. A symmetrization step is therefore applied, for example by averaging upper and lower triangular entries. If necessary, the resulting matrix can be projected to the cone of symmetric positive definite matrices to ensure validity.

After discarding an initial burn-in period, posterior summaries such as the mean and median precision matrices are computed as

$$\hat{\Omega}_{\text{mean}} = \frac{1}{n_{\text{keep}}} \sum_{t \in \text{kept}} \Omega^{(t)}, \quad \hat{\Omega}_{\text{median}} = \text{median}_{t \in \text{kept}} \Omega^{(t)}.$$

2.4.3 Initialization and practical considerations

Latent Z is initialized by setting $Z_{ij} = Y_{ij}$ when uncensored, and $Z_{ij} = c_j - \epsilon_{ij}$ for censored entries with $\epsilon_{ij} \sim |\mathcal{N}(0, 1)|$. Regression parameters are initialized at neutral values ($\theta_j = 0$, $\sigma_j^2 = 1$, $\lambda_{jk}^2 = \nu_{jk} = \tau_j^2 = \xi_j = 1$). Default hyperparameters $(a_0, b_0) = (10^{-2}, 10^{-2})$ provide weakly informative priors for variance terms, while the hierarchical horseshoe prior adaptively shrinks small coefficients without overshrinking large signals. Efficient truncated normal sampling relies on stable implementations of the inverse-cdf method, with exponential tilting for extreme truncation. Linear algebra computations use Cholesky factorization of A , with Gaussian sampling via $\theta_j = \mu_\theta + \sigma_j L^{-\top} U$ where $LL^\top = A$ and $U \sim \mathcal{N}(0, I)$.

2.5 Extension to right-censored data

Extension to right-censored data is similar, that is rather focus on $(-\infty, c]$, we use $[c, \infty)$. Formally, the conditional distribution takes the form

$$Z_{ij} \mid \tilde{Y}_{ij}, \Omega, Z_{i,-j} \sim \begin{cases} \mathcal{N}(\mu_{ij}, \sigma_j^2), & \text{if } \tilde{Y}_{ij} = Z_{ij}, \\ \mathcal{N}(\mu_{ij}, \sigma_j^2) \mathbb{I}(Z_{ij} \geq c_j), & \text{if } \tilde{Y}_{ij} = c_j, \end{cases}$$

Thus, (4) is replaced by

$$Z_{ij} \sim \mathcal{N}(\mu_{ij}, \sigma_j^2) \text{ restricted to } [c_j, \infty). \quad (5)$$

and the other step of the algorithm remain unchanged.

3 Graphical Horseshoe with Missing Data

3.1 Model setup and prior specification

Consider an i.i.d. sample $Y = (Y_1, \dots, Y_n) \in \mathbb{R}^{n \times p}$ from a p -dimensional Gaussian distribution with mean zero and precision matrix $\Omega \succ 0$. In practice, many data sets of this type contain missing values. Let $\mathcal{O} \subseteq \{1, \dots, n\} \times \{1, \dots, p\}$ denote the set of observed entries and $\mathcal{M} = \mathcal{O}^c$ the set of missing entries. For $(i, j) \in \mathcal{O}$ we observe \tilde{Y}_{ij} , while values in \mathcal{M} remain unobserved. The inferential goal is to recover the sparse precision matrix Ω under such incomplete data.

Throughout, we assume the data are missing at random, in the sense that the probability of missingness depends only on observed variables and not on the unobserved values themselves. Under this assumption, the missingness mechanism can be ignored for likelihood-based inference, which allows us to formulate a Bayesian estimation procedure through data augmentation.

The observed-data likelihood is obtained by marginalizing over the missing components of each Y_i . Writing \mathcal{O}_i for the set of observed coordinates in row i , the distribution of \tilde{Y}_i is multivariate Gaussian with mean zero and covariance matrix given by the corresponding principal submatrix of $\Sigma = \Omega^{-1}$. Hence,

$$L(\Omega; \{\tilde{Y}_i\}_{i=1}^n) = \prod_{i=1}^n p(\tilde{Y}_i \mid \Omega),$$

with $\tilde{Y}_i \sim \mathcal{N}_{|\mathcal{O}_i|}(0, \Sigma_{\mathcal{O}_i, \mathcal{O}_i})$. Equivalently, the likelihood admits the form

$$L(\Omega; \tilde{Y}) = \prod_{i=1}^n (2\pi)^{-|\mathcal{O}_i|/2} |\Sigma_{\mathcal{O}_i, \mathcal{O}_i}|^{-1/2} \exp\left(-\frac{1}{2} \tilde{Y}_i^\top \Sigma_{\mathcal{O}_i, \mathcal{O}_i}^{-1} \tilde{Y}_i\right), \quad (6)$$

where $\Sigma = \Omega^{-1}$. This representation emphasizes that only the observed entries contribute to the likelihood, while the unobserved entries are integrated out.

Here, we use the same graphical Horseshoe prior as in the previous section, given in (3).

3.2 Posterior computation via Gibbs sampling

Posterior inference under the graphical Horseshoe prior with missing data is performed via a Gibbs sampling algorithm. The sampler alternates between imputing missing entries of the latent Gaussian matrix and updating the precision matrix under the graphical Horseshoe prior.

3.2.1 Initialization

The Gibbs sampler begins with initial values for both the latent data matrix Z and the precision matrix Ω . For the missing entries, simple imputations such as column means or draws from a Gaussian fitted to the observed components of each variable provide reasonable starting values. The initial matrix is therefore

$$Z_{ij}^{(0)} = \begin{cases} \tilde{Y}_{ij}, & (i, j) \in \mathcal{O}, \\ \text{imputed value}, & (i, j) \in \mathcal{M}. \end{cases}$$

The precision matrix Ω must be initialized as a symmetric positive definite matrix. The identity matrix is the simplest choice, while a ridge-regularized inverse covariance estimate can yield faster convergence. In all cases, the initialization must satisfy $\Omega^{(0)} \succ 0$.

3.2.2 Imputation of missing values

At each iteration, missing entries in Z are resampled from their conditional Gaussian distributions given the observed components and the current covariance estimate. Let $\Sigma^{(t-1)} = (\Omega^{(t-1)})^{-1}$ and partition it into blocks corresponding to observed indices o and missing indices m for a given row i . The conditional mean and covariance of the missing values are

$$\mu_m = \Sigma_{mo} \Sigma_{oo}^{-1} Z_{i,o}, \quad \Sigma_m = \Sigma_{mm} - \Sigma_{mo} \Sigma_{oo}^{-1} \Sigma_{om}.$$

The missing entries are then imputed as

$$Z_{i,m} \sim \mathcal{N}(\mu_m, \Sigma_m).$$

3.2.3 Nodewise regression updates

With the full latent data matrix Z in hand, the precision matrix is updated through nodewise regressions under the graphical Horseshoe prior, as in Section 2.4. We omit repeating the same here for the sake of brevity.

The completed latent data matrix Z is simultaneously available, offering a coherent Bayesian framework that unifies imputation and sparse graphical modeling in high-dimensional Gaussian settings.

4 Numerical studies

Our methods for both cases of censored and missing data are implemented in the R package `GHScenmis` available on Github: <https://github.com/tienmt/ghscenmis>.

4.1 Simulation setup and compared methods

We compare our proposed methods against the Lasso approach tailored for censored and missing data as in [3, 39], with software implementations available through the R package `cglasso` [4]. Our Gibbs samplers are run with 5000 samples, with initial 1000 samples as burn-in. The `cglasso` method is run with default options and its tuning parameter is selected via AIC information criteria.

We consider two settings for generating the true precision matrix (Ω_{true}) and the corresponding covariance matrix (Σ_{true}) in our simulation study.

Setting 1: Tridiagonal Precision Matrix.

In the first scenario, we construct a tridiagonal precision matrix with off-diagonal elements representing

weak conditional dependence between adjacent variables. Formally, let p denote the number of variables, and define a $p \times p$ matrix A with

$$A_{ij} = \begin{cases} 0.3, & \text{if } |i - j| = 1 \\ 0, & \text{otherwise} \end{cases}$$

The true precision matrix is then $\Omega_{\text{true}} = \text{diag}(1, \dots, 1) + A$. The corresponding covariance matrix is obtained by matrix inversion: $\Sigma_{\text{true}} = \Omega_{\text{true}}^{-1}$. This structure mimics a simple chain graph where each variable depends on its immediate neighbors.

Setting 2: Small Fully Connected Subset.

In the second scenario, we introduce a small, densely connected subset of variables to study the effect of moderate correlations among a few variables. We define the covariance matrix Σ_{true} as the identity matrix with added off-diagonal entries of 0.5 among the first three variables:

$$\Sigma_{\text{true}} = \begin{pmatrix} 1 & 0.5 & 0.5 & 0 & \cdots & 0 \\ 0.5 & 1 & 0.5 & 0 & \cdots & 0 \\ 0.5 & 0.5 & 1 & 0 & \cdots & 0 \\ 0 & 0 & 0 & 1 & & 0 \\ \vdots & \vdots & \vdots & & \ddots & \vdots \\ 0 & 0 & 0 & 0 & \cdots & 1 \end{pmatrix}.$$

The corresponding precision matrix is then computed as $\Omega_{\text{true}} = \Sigma_{\text{true}}^{-1}$, which is still a very sparse matrix. This setting allows us to examine estimation performance in the presence of a small but strong correlation block, contrasting with the sparse tridiagonal structure in Setting 1.

We evaluate each estimate from a method, $\widehat{\Omega}$, by considering squared ℓ_2 norm error, given as $\|\widehat{\Omega} - \Omega_{\text{true}}\|_2^2$. Each simulation setup is repeated 100 times.

4.2 Simulations results with censored data

We begin by presenting simulation studies in which the data are censored under a wide variety of scenarios.

Results with increasing dimensions. We set the sample size to $n = 200$ and vary the dimension $p \in \{10, 20, 30\}$. Data are generated from a multivariate Gaussian distribution with the true precision matrix corresponding to either Setting I or Setting II (as described above). The generated data are then left-censored at the fixed threshold $c = (-0.5, 0.5, -0.5, 0.5, \dots, -0.5, 0.5)$. This procedure is repeated 100 times, and the resulting estimation errors are summarized using in Table 1.

The results show a clear trend: as the dimension increases, both HScen and the censored graphical Lasso (cglasso) exhibit larger errors. Nevertheless, our Bayesian method consistently achieves smaller errors, highlighting its advantage in high-dimensional censored settings.

Results with increasing proportion of data being censored. We next consider the case with fixed sample size $n = 200$ and dimension $p = 10$. Instead of applying censoring at a fixed vector, we examine the impact of censoring at different proportions: 10%, 20%, and 30% of the data. Specifically, data are generated from a multivariate Gaussian distribution with the true precision matrix given by either Setting I or Setting II (as described above), and censoring is applied at the empirical quantiles corresponding to the desired proportions. The procedure is repeated 100 times, and the resulting estimation errors are summarized in Table 2.

The results indicate that both HScen and cglasso are affected by the degree of censoring. Nevertheless, our Bayesian method HScen consistently outperforms cglasso across all scenarios, with the performance gap becoming particularly pronounced when 50% of the data are censored.

Table 1: Simulation results with increasing dimensions (the number of variables) for censored data with $n = 200$, with censored vector is fixed at $c = (-0.5, 0.5, \dots, -0.5, 0.5)$. TPR: true positive rate and FDR: false positive rate.

Method	$\ \hat{\beta} - \beta_0\ _2^2$	TPR	FDR	$\ \hat{\beta} - \beta_0\ _2^2$	TPR	FDR
	Setting I, $p = 10$				Setting II, $p = 10$	
cgLasso	2.13 (0.21)	0.00 (0.01)	0.00 (0.00)	1.91 (2.02)	1.00 (0.00)	0.59 (0.40)
cenGHS	0.65 (0.23)	0.82 (0.11)	0.01 (0.02)	0.65 (0.38)	0.92 (0.15)	0.00 (0.01)
	Setting I, $p = 20$				Setting II, $p = 20$	
cgLasso	4.44 (0.19)	0.00 (0.01)	0.00 (0.00)	2.44 (2.47)	1.00 (0.03)	0.27 (0.35)
cenGHS	1.60 (0.42)	0.71 (0.10)	0.01 (0.01)	0.96 (0.37)	0.87 (0.16)	0.00 (0.00)
	Setting I, $p = 30$				Setting II, $p = 30$	
cgLasso	6.69 (0.26)	0.00 (0.01)	0.00 (0.00)	3.04 (4.63)	1.00 (0.03)	0.11 (0.26)
cenGHS	2.53 (0.44)	0.61 (0.10)	0.00 (0.00)	1.42 (0.75)	0.79 (0.16)	0.00 (0.00)

Table 2: Simulation results for censored data with $n = 200, p = 10$, with increasing the amount of data being censored from 10%, 20%, and 30% . TPR: true positive rate and FDR: false positive rate.

Method	$\ \hat{\beta} - \beta_0\ _2^2$	TPR	FDR	$\ \hat{\beta} - \beta_0\ _2^2$	TPR	FDR
	Setting I, 10% censored				Setting II, 10% censored	
cgLasso	0.45 (0.34)	1.00 (0.00)	0.51 (0.24)	0.41 (0.19)	1.00 (0.00)	0.28 (0.15)
cenGHS	0.38 (0.13)	0.99 (0.04)	0.03 (0.03)	0.39 (0.18)	0.99 (0.05)	0.01 (0.02)
	Setting I, 20% censored				Setting II, 20% censored	
cgLasso	0.54 (0.26)	1.00 (0.00)	0.62 (0.29)	0.55 (0.41)	1.00 (0.00)	0.43 (0.29)
cenGHS	0.41 (0.14)	0.98 (0.04)	0.04 (0.03)	0.42 (0.18)	1.00 (0.03)	0.01 (0.02)
	Setting I, 30% censored				Setting II, 30% censored	
cgLasso	0.66 (0.22)	0.99 (0.03)	0.54 (0.35)	0.87 (0.60)	1.00 (0.00)	0.62 (0.35)
cenGHS	0.46 (0.14)	0.96 (0.06)	0.03 (0.03)	0.46 (0.23)	0.97 (0.09)	0.01 (0.02)

Results with increasing sample size. We next investigate the effect of increasing the sample size on estimation accuracy. The dimension is fixed at $p = 10$, and censoring is applied at the fixed vector $(-0.5, 0.5, -0.5, 0.5, \dots, -0.5, 0.5)$. Sample sizes are varied across $n = 200, 500, 1000$. Data are generated from a multivariate Gaussian distribution with the true precision matrix corresponding to either Setting I or Setting II (as described above). Results over 100 replications are summarized in Table 3.

As expected, both HScen and cglasso show reduced estimation error as the sample size increases. However, the Bayesian method HScen demonstrates a clear advantage, achieving substantially smaller errors, particularly at larger sample sizes. Moreover, cglasso performs poorly under Setting I, where the underlying graph structure follows a chain, further highlighting the robustness of our approach.

4.3 Simulations with missing data

Results with increasing dimensions. We fix the sample size at $n = 200$ and vary the dimension $p \in \{10, 20, 30\}$. Data are generated from a multivariate Gaussian distribution with the true precision matrix specified by either Setting I or Setting II (as described above). To mimic missingness, 10% of the simulated observations are removed uniformly at random. This procedure is repeated 100 times, and the resulting estimation errors are displayed as in Table 4.

The results show that the estimation errors of both methods increase with dimension. Nonetheless, the Bayesian method HScen consistently achieves smaller errors than cglasso, with the performance gap being most pronounced when the true precision matrix corresponds to Setting II.

Table 3: Simulation results with increasing the sample sizes for censored data with $p = 10$, with censored vector is fixed at $c = (-0.5, 0.5, \dots, -0.5, 0.5)$. TPR: true positive rate and FDR: false positive rate.

Method	$\ \hat{\beta} - \beta_0\ _2^2$	TPR	FDR	$\ \hat{\beta} - \beta_0\ _2^2$	TPR	FDR
	Setting I, $n = 200$				Setting II, $n = 200$	
cgLasso	2.13 (0.21)	0.00 (0.01)	0.00 (0.00)	1.91 (2.02)	1.00 (0.00)	0.59 (0.40)
cenGHS	0.65 (0.23)	0.82 (0.11)	0.01 (0.02)	0.65 (0.38)	0.92 (0.15)	0.00 (0.01)
	Setting I, $n = 500$				Setting II, $n = 500$	
cgLasso	2.01 (0.09)	0.00 (0.00)	0.00 (0.00)	1.00 (0.63)	1.00 (0.00)	0.72 (0.41)
cenGHS	0.24 (0.08)	1.00 (0.00)	0.02 (0.02)	0.21 (0.10)	1.00 (0.00)	0.01 (0.01)
	Setting I, $n = 1000$				Setting II, $n = 1000$	
cgLasso	1.97 (0.08)	0.04 (0.15)	0.00 (0.00)	0.82 (0.51)	1.00 (0.00)	0.76 (0.41)
cenGHS	0.11 (0.03)	1.00 (0.00)	0.02 (0.02)	0.10 (0.05)	1.00 (0.00)	0.01 (0.01)

Table 4: Simulation results for 10% missing data with $n = 200$ and increase dimension. TPR: true positive rate and FDR: false discovery rate.

Method	$\ \hat{\beta} - \beta_0\ _2^2$	TPR	FDR	$\ \hat{\beta} - \beta_0\ _2^2$	TPR	FDR
	Setting I, $p = 10$				Setting II, $p = 10$	
cgLasso	0.62 (0.37)	1.00 (0.00)	0.66 (0.30)	0.45 (0.30)	1.00 (0.00)	0.34 (0.20)
cenGHS	0.38 (0.12)	0.96 (0.06)	0.02 (0.03)	0.37 (0.17)	0.97 (0.09)	0.01 (0.01)
	Setting I, $p = 20$				Setting II, $p = 20$	
cgLasso	0.93 (0.14)	1.00 (0.00)	0.42 (0.07)	0.71 (0.20)	1.00 (0.00)	0.09 (0.09)
cenGHS	0.91 (0.18)	0.90 (0.07)	0.01 (0.01)	0.58 (0.23)	0.95 (0.12)	0.00 (0.00)
	Setting I, $p = 30$				Setting II, $p = 30$	
cgLasso	1.66 (0.20)	1.00 (0.01)	0.33 (0.12)	0.98 (0.21)	1.00 (0.00)	0.03 (0.04)
cenGHS	1.42 (0.25)	0.85 (0.07)	0.00 (0.00)	0.78 (0.31)	0.92 (0.15)	0.00 (0.00)

Results with increasing sample size. We next examine how increasing the sample size affects estimation accuracy. The dimension is fixed at $p = 10$, and sample sizes are set to $n = 200, 500, 1000$. Data are generated from a multivariate Gaussian distribution with the true precision matrix corresponding to either Setting I or Setting II (as described above), after which 10% of the data are removed uniformly at random. Results over 100 replications are presented in Tables 5.

As expected, both methods achieve lower errors as the sample size increases. However, the Bayesian approach HScen consistently outperforms cglasso across all scenarios, demonstrating superior robustness to missing data.

Results with increasing proportion of missing data. We now fix the sample size at $n = 200$ and dimension at $p = 10$, and investigate the effect of varying the proportion of missing data. Specifically, we consider missingness levels of 10%, 20%, and 30%. Data are generated from a multivariate Gaussian distribution with the true precision matrix corresponding to either Setting I or Setting II (as described above). The specified proportion of entries is then removed uniformly at random. This process is repeated 100 times, and the resulting estimation errors are displayed as in Table 6.

As expected, both methods exhibit a modest increase in estimation error as the proportion of missing data rises. Nevertheless, the Bayesian method cenGHS consistently outperforms cglasso, yielding smaller and more stable errors across all levels of missingness.

Some trace and acf plots are given in Appendix A together with effective sample size of the MCMC samples to demonstrate the behavior of the algorithm.

Table 5: Simulation results for 10% missing data with $p = 10$ increase sample size. TPR: true positive rate and FDR: false discovery rate.

Method	$\ \hat{\beta} - \beta_0\ _2^2$	TPR	FDR	$\ \hat{\beta} - \beta_0\ _2^2$	TPR	FDR
Setting I, $n = 200$						
cgLasso	0.62 (0.37)	1.00 (0.00)	0.66 (0.30)	0.45 (0.30)	1.00 (0.00)	0.34 (0.20)
cenGHS	0.38 (0.12)	0.96 (0.06)	0.02 (0.03)	0.37 (0.17)	0.97 (0.09)	0.01 (0.01)
Setting I, $n = 500$						
cgLasso	0.27 (0.08)	1.00 (0.00)	0.86 (0.29)	0.19 (0.12)	1.00 (0.00)	0.28 (0.24)
cenGHS	0.14 (0.05)	1.00 (0.00)	0.03 (0.03)	0.14 (0.06)	1.00 (0.00)	0.01 (0.02)
Setting I, $n = 1000$						
cgLasso	0.13 (0.03)	1.00 (0.00)	1.00 (0.00)	0.17 (0.05)	1.00 (0.00)	0.58 (0.46)
cenGHS	0.07 (0.02)	1.00 (0.00)	0.03 (0.03)	0.07 (0.03)	1.00 (0.00)	0.01 (0.02)

Table 6: Simulation results for censored data with $n = 200, p = 20$, with increasing the amount of data being censored from 10%, 20%, and 30% . TPR: true positive rate and FDR: false positive rate.

Method	$\ \hat{\beta} - \beta_0\ _2^2$	TPR	FDR	$\ \hat{\beta} - \beta_0\ _2^2$	TPR	FDR
Setting I, missing 10%						
cgLasso	0.93 (0.14)	1.00 (0.00)	0.42 (0.07)	0.71 (0.20)	1.00 (0.00)	0.09 (0.09)
cenGHS	0.91 (0.18)	0.90 (0.07)	0.01 (0.01)	0.58 (0.23)	0.95 (0.12)	0.00 (0.00)
Setting I, missing 20%						
cgLasso	1.65 (1.24)	1.00 (0.01)	0.53 (0.22)	0.89 (0.22)	1.00 (0.00)	0.08 (0.11)
cenGHS	1.15 (0.21)	0.75 (0.09)	0.00 (0.00)	0.67 (0.31)	0.90 (0.15)	0.00 (0.00)
Setting I, missing 30%						
cgLasso	1.94 (0.78)	0.99 (0.02)	0.61 (0.26)	1.17 (0.26)	0.99 (0.06)	0.05 (0.06)
cenGHS	1.71 (0.26)	0.49 (0.10)	0.00 (0.00)	0.81 (0.30)	0.72 (0.16)	0.00 (0.00)

5 Application to single cell-data: megakaryocyte-erythroid progenitors

In a study of blood cell formation, Psaila et al. [36] identified three distinct sub-populations of cells derived from hematopoietic stem cells through differentiation. One of these sub-populations, termed MK-MEP, is a previously uncharacterized, rare population of bipotent cells that primarily give rise to megakaryocytic progeny. The data is available from the `cgllasso` package

Multiplex RT-qPCR was used to profile the expression of 63 genes across 48 single human MK-MEP cells. RT-qPCR measurements are typically right-censored, with a manufacturer-specified detection limit of 40 (the censored level). Raw expression values were mean-normalized following the approach of Pipelers et al. [34]. Further details are provided in Augugliaro et al. [3].

We applied the GHScen method for 10,000 iterations, discarding the first 1,000 iterations as burn-in. Figure 1 shows the estimated graphs obtained from different methods. For GHScen, nonzero entries in the precision matrix were identified using 95% credible intervals that do not include zero. Compared with cgllasso, the graph estimated by GHScen is notably sparser and reveals five distinct connected subgroups, whereas cgllasso produces a single large connected component.

6 Theoretical results

In this section, we study posterior contraction of the tempered (o, fractional) posterior for the proposed censored Graphical Horseshoe in high-dimensional Gaussian graphical models with missing or censored

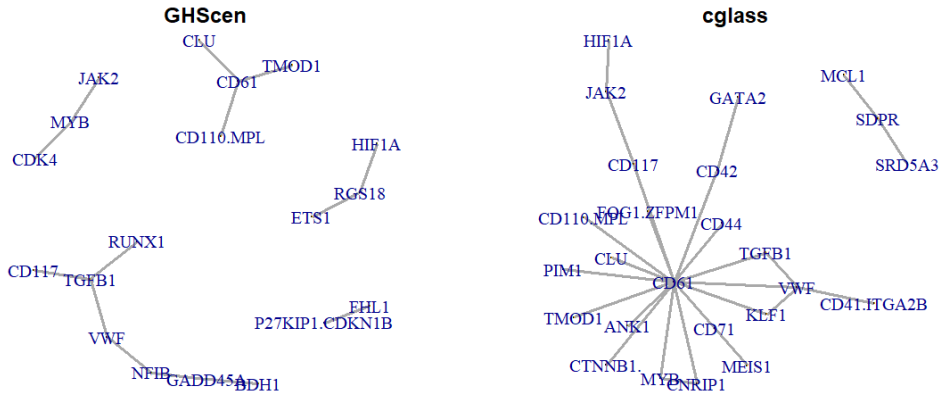


Figure 1: Graphs from different methods on the real data set MKMEP. We see that GHSsen return a sparse networks compared to cglasso.

observations. The main technical difficulty arises from the observed-data likelihood: missingness leads to marginal Gaussian likelihoods, while censoring introduces non-linear log-CDF terms that distort curvature and preclude global log-concavity. We show that, despite these complications, the global-local shrinkage structure of the graphical Horseshoe prior yields sharp posterior concentration under standard sparsity and spectral regularity conditions.

Our analysis is conducted in terms of Rényi divergence, which provides a natural information-theoretic loss for tempered posteriors and remains well suited to likelihoods with non-quadratic structure. The results demonstrate that the posterior concentrates around the true precision matrix at the same order as in fully observed Gaussian graphical models, up to constants depending on the censoring mechanism.

Let p_Ω and P_Ω denote the density and the distribution of a Gaussian $\mathcal{N}(0, \Omega^{-1})$ random variable. Denoting the prior on Ω by $\pi_{HS}(\Omega)$, the tempered posterior [8, 1, 25, 29] is given by

$$\pi_{n,\alpha}(\Omega) \propto L^\alpha(\Omega; \tilde{Y}) \pi_{HS}(\Omega).$$

We consider the following assumptions regarding the truth.

Assumption 1 (Bounded spectrum). *The precision matrix Ω, Ω_0 lie in the spectral band*

$$\mathcal{S} = \{\Omega \succ 0 : 0 < m \leq \lambda_{\min}(\Omega) \leq \lambda_{\max}(\Omega) \leq M < \infty\}.$$

Assumption 2. *The true precision matrix Ω_0 is sparse in the sense that*

$$\Omega_0 \in \mathcal{S}(s) := \left\{ \Omega \in \mathcal{S} : \sum_{1 \leq i < j \leq p} \mathbf{1}_{(\omega_{ij} \neq 0)} \leq s, s < n \right\}.$$

Assumption 3 (Non-degenerate censoring probability.). *There exists a finite constant $K_1 = K_1(m, M, c)$ such that for every $\Omega_t \in \mathcal{S}$ and every matrix $A \in \mathbb{R}^{p \times p}$, the following quadratic form involving the expected Hessian is bounded:*

$$|\text{trace}(A^\top \mathbb{E}_{\Omega_0} [\nabla^2 \ell(\Omega_t; \tilde{Y})] A)| \leq K_1 \|A\|_F^2.$$

Assumption 1 is standard in both frequentist and Bayesian literature for sparse precision matrix estimation, [10, 19, 6, 38, 42]. The sparsity condition in Assumption 2 is common in high-dimensional settings [7, 18, 5]. Assumption 3 is a non-trivial assumption for censored data due to the log-CDF term in the likelihood. Its role is to control the local curvature of the observed-data log-likelihood, which, due to censoring, contains Gaussian distribution function terms rather than purely quadratic forms. These terms destroy global log-concavity and can, in principle, lead to regions of near-flat likelihood. The assumption

requires that the expected Hessian of the censored log-likelihood remains uniformly bounded in Frobenius norm over a spectral neighborhood of the truth. This condition ensures that the information loss induced by censoring is controlled and that the likelihood retains sufficient local identifiability to support posterior concentration. In particular, it rules out degenerate censoring configurations in which large portions of the data contribute negligible information about the precision matrix.

From a statistical perspective, Assumption 3 can be interpreted as an information non-degeneracy condition: it guarantees that censoring does not eliminate curvature in directions corresponding to nonzero precision matrix entries. Similar curvature or restricted eigenvalue conditions are implicitly required in frequentist analyses of censored graphical models, although they are rarely stated explicitly. Here, the assumption allows the Bayesian posterior to concentrate at the same rate as in the fully observed case, up to constants depending on the censoring thresholds.

We now present first a consistency result of the tempered posterior in $p > n$ setting.

Given two probability measures, P and R , that are both dominated by a shared measure ν , and for any α in $(0, 1)$, the α -Rényi divergence between P and R is given by the formula:

$$\mathcal{D}_\alpha(P, R) = \frac{1}{\alpha - 1} \log \int \left(\frac{dP}{d\nu} \right)^\alpha \left(\frac{dR}{d\nu} \right)^{1-\alpha} d\nu.$$

Furthermore, the Kullback-Leibler divergence is defined as $\mathcal{K}(P, R) = \int \log \left(\frac{dP}{dR} \right) dP$. This definition holds provided that P is absolutely continuous with respect to R (denoted $P \ll R$). If this condition is not met, the divergence is taken to be $+\infty$. We now present the results on posterior contraction for the case of censored data, followed by the same for missing data.

Theorem 1 (Posterior contraction for censored data). *Consider the model formulation for censored data as in Section 2. For any $\alpha \in (0, 1)$, under Assumptions 1, 2, 3, we have that*

$$\mathbb{E} \left[\int \mathcal{D}_\alpha(P_\Omega, P_{\Omega_0}) \pi_{n,\alpha}(d\Omega) \right] \leq \frac{1+\alpha}{1-\alpha} \varepsilon_n.$$

with $\varepsilon_n = Kn^{-1}s \log p$, for some universal constant $K > 0$ depending only on m, M and the censored value c .

Theorem 2 (Posterior contraction for missing data). *Consider the model formulation for missing data as in Section 3. For any $\alpha \in (0, 1)$, under Assumptions 1, 2, we have that*

$$\mathbb{E} \left[\int \mathcal{D}_\alpha(P_\Omega, P_{\Omega_0}) \pi_{n,\alpha}(d\Omega) \right] \leq \frac{1+\alpha}{1-\alpha} \varepsilon_n.$$

with $\varepsilon_n = Kn^{-1}s \log p$, for some universal constant $K > 0$ does not depending on n, p, s .

Discussion of the results. Theorems 1 and 2 establish that, for both missing and censored data, the tempered posterior contracts at rate $\varepsilon_n \asymp n^{-1}s \log p$, which coincides with the optimal rate for sparse precision matrix estimation under complete observation [38]. Thus, incomplete observation does not fundamentally alter the statistical difficulty of the problem.

The distinction between the two regimes lies in likelihood geometry. For missing data, contraction follows from standard Kullback–Leibler control after marginalization. For censored data, additional regularity is required to control the curvature of the log-likelihood induced by Gaussian CDF terms.

Importantly, the results are adaptive: the contraction rate depends on the unknown sparsity level s , with no tuning of the Horseshoe prior. This confirms that global-local shrinkage remains theoretically stable under censoring and missingness. To our knowledge, these are the first posterior contraction results for sparse precision matrix estimation in the presence of censoring; comparable guarantees are currently unavailable for penalized likelihood methods such as the censored graphical lasso.

7 Discussion and conclusion

This work extends Bayesian precision matrix estimation to settings involving censored and missing (high-dimensional) Gaussian data by introducing the Censored Graphical Horseshoe (CGHS) model. Building on the adaptive shrinkage properties of the graphical Horseshoe prior, our formulation incorporates a latent-variable representation that naturally handles censored observations as well as arbitrarily missing entries. This generalization substantially broadens the applicability of the Horseshoe framework, enabling principled inference in problems where existing graphical modeling tools are not directly equipped to handle incomplete or censored measurements.

A key contribution of our paper is the development of an efficient Gibbs sampling algorithm for posterior computation. By alternating between imputing latent data, updating regression coefficients and error variances, adapting local and global shrinkage scales, and reconstructing the precision matrix, the sampler provides a tractable route to full Bayesian inference in models that would otherwise be computationally prohibitive.

Perhaps the most distinctive aspect of this work is the theoretical analysis. We derive posterior concentration rates for both censored-data and missing-data regimes, establishing that CGHS recovers the underlying precision structure at near-optimal rates under standard sparsity conditions. To the best of our knowledge, no analogous results exist for frequentist or Bayesian versions of the graphical lasso in these regimes. Our theory therefore fills an important gap in the literature, demonstrating that global-local shrinkage priors remain stable and adaptively informative even when the likelihood is distorted by censoring or incomplete observations.

There are several promising avenues for future work. One direction is to extend CGHS beyond the Gaussian setting—for example, to copula-based or semiparametric graphical models—which would broaden its applicability to non-normal data structures. Another is to develop scalable posterior approximation methods, such as variational inference or stochastic-gradient MCMC, to improve computational efficiency in ultra-high-dimensional domains like genomics and neuroimaging. Incorporating Missing Not at Random (MNAR) mechanisms into the latent-variable framework represents an additional challenge with substantial practical relevance, particularly in biomedical studies where the missingness may depend on unobserved values. Finally, establishing formal model-selection strategies or credible-graph procedures would enable principled uncertainty quantification for inferred network structures.

Acknowledgments

The views, findings, and opinions presented in this work are exclusively those of the authors and do not reflect the official stance of the Norwegian Institute of Public Health or IIM Indore.

Conflicts of interest/Competing interests

The authors declare no potential conflict of interests.

References

- [1] Alquier, P. and Ridgway, J. (2020). Concentration of tempered posteriors and of their variational approximations. *The Annals of Statistics*, 48(3):1475–1497.
- [2] Atchadé, Y. F. (2019). Quasi-bayesian estimation of large gaussian graphical models. *Journal of Multivariate Analysis*, 173:656–671.
- [3] Augugliaro, L., Abbruzzo, A., and Vinciotti, V. (2020). ℓ_1 -penalized censored gaussian graphical model. *Biostatistics*, 21(2):e1–e16.

- [4] Augugliaro, L., Sottile, G., Wit, E. C., and Vinciotti, V. (2023). cglasso: An r package for conditional graphical lasso inference with censored and missing values. *Journal of Statistical Software*, 105:1–58.
- [5] Banerjee, S., Castillo, I., and Ghosal, S. (2021). Bayesian inference in high-dimensional models. *arXiv preprint arXiv:2101.04491*.
- [6] Banerjee, S. and Ghosal, S. (2015). Bayesian structure learning in graphical models. *Journal of Multivariate Analysis*, 136:147–162.
- [7] Bellec, P. C., Lecu , G., and Tsybakov, A. B. (2018). Slope meets lasso: improved oracle bounds and optimality. *The Annals of Statistics*, 46(6B):3603–3642.
- [8] Bhattacharya, A., Pati, D., and Yang, Y. (2019). Bayesian fractional posteriors. *Annals of Statistics*, 47(1):39–66.
- [9] Cai, T., Liu, W., and Luo, X. (2011). A constrained l-1 minimization approach to sparse precision matrix estimation. *Journal of the American Statistical Association*, 106(494):594–607.
- [10] Cai, T. T., Ren, Z., and Zhou, H. H. (2016). Estimating structured high-dimensional covariance and precision matrices: Optimal rates and adaptive estimation. *Electronic Journal of Statistics*, 10:1–59.
- [11] Callot, L., Caner, M.,  nder, A.  ., and Ula an, E. (2021). A nodewise regression approach to estimating large portfolios. *Journal of Business & Economic Statistics*, 39(2):520–531.
- [12] Carvalho, C. M., Polson, N. G., and Scott, J. G. (2010). The horseshoe estimator for sparse signals. *Biometrika*, pages 465–480.
- [13] Derveaux, S., Vandesompele, J., and Hellemans, J. (2010). How to do successful gene expression analysis using real-time pcr. *Methods*, 50(4):227–230.
- [14] Fan, J., Feng, Y., and Wu, Y. (2009). Network exploration via the adaptive lasso and scad penalties. *Annals of Applied Statistics*, 3(2):521–541.
- [15] Fan, J., Liao, Y., and Liu, H. (2016). An overview of the estimation of large covariance and precision matrices. *The Econometrics Journal*, 19(1):C1–C32.
- [16] Friedman, J., Hastie, T., and Tibshirani, R. (2008). Sparse inverse covariance estimation with the graphical lasso. *Biostatistics*, 9(3):432–441.
- [17] Gan, L., Narisetty, N. N., and Liang, F. (2019). Bayesian regularization for graphical models with unequal shrinkage. *Journal of the American Statistical Association*, 114(527):1218–1231.
- [18] Gao, C., van der Vaart, A. W., and Zhou, H. H. (2020). A general framework for bayes structured linear models. *Annals of Statistics*, 48(5):2848–2878.
- [19] Jankov , J. and van de Geer, S. (2017). Honest confidence regions and optimality in high-dimensional precision matrix estimation. *Test*, 26:143–162.
- [20] Lauritzen, S. L. (1996). *Graphical Models*. Oxford University Press.
- [21] Li, Y., Craig, B. A., and Bhadra, A. (2019). The graphical horseshoe estimator for inverse covariance matrices. *Journal of Computational and Graphical Statistics*, 28(3):747–757.
- [22] Lounici, K. (2014). High-dimensional covariance matrix estimation with missing observations. *Bernoulli*, 20(3):1029–1058.

[23] Mai, T. T. (2024). Concentration of a Sparse Bayesian Model With Horseshoe Prior in Estimating High-Dimensional Precision Matrix. *Stat*, 13(4):e70008.

[24] Mai, T. T. (2025a). Adaptive posterior concentration rates for sparse high-dimensional linear regression with random design and unknown error variance. *Journal of the Korean Statistical Society*, pages 1–35.

[25] Mai, T. T. (2025b). Concentration properties of fractional posterior in 1-bit matrix completion. *Machine Learning*, 114(1):7.

[26] Mai, T. T. (2025c). Handling bounded response in high dimensions: a horseshoe prior bayesian beta regression approach. *arXiv preprint arXiv:2505.22211*.

[27] Mai, T. T. (2025d). High-dimensional bayesian tobit regression for censored response with horseshoe prior. *arXiv preprint arXiv:2505.08288*.

[28] Mai, T. T. (2025e). On high-dimensional classification by sparse generalized bayesian logistic regression. *Statistical Papers*.

[29] Mai, T. T. (2025f). On properties of fractional posterior in generalized reduced-rank regression. *Journal of Multivariate Analysis*, page 105481.

[30] Mai, T. T. (2025g). A sparse pac-bayesian approach for high-dimensional quantile prediction. *Statistics and Computing*, 35(4):93.

[31] McCall, M. N., McMurray, H. R., Land, H., and Almudevar, A. (2014). On non-detects in qPCR data. *Bioinformatics*, 30(16):2310–2316.

[32] Meinshausen, N. and Bühlmann, P. (2006). Variable selection and high-dimensional graphs with the lasso. *Annals of Statistics*, 34:1436–1462.

[33] Pesonen, M., Pesonen, H., and Nevalainen, J. (2015). Covariance matrix estimation for left-censored data. *Computational Statistics & Data Analysis*, 92:13–25.

[34] Pipelers, P., Clement, L., Vynck, M., Hellemans, J., Vandesompele, J., and Thas, O. (2017). A unified censored normal regression model for qPCR differential gene expression analysis. *Plos one*, 12(8):e0182832.

[35] Pourahmadi, M. (2011). Covariance estimation: The glm and regularization perspectives. *Statistical Science*, 26(3):369–387.

[36] Psaila, B., Barkas, N., Iskander, D., Roy, A., Anderson, S., Ashley, N., Caputo, V. S., Lichtenberg, J., Loaiza, S., Bodine, D. M., et al. (2016). Single-cell profiling of human megakaryocyte-erythroid progenitors identifies distinct megakaryocyte and erythroid differentiation pathways. *Genome biology*, 17(1):83.

[37] Ryali, S., Chen, T., Supekar, K., and Menon, V. (2012). Estimation of functional connectivity in fMRI data using stability selection-based sparse partial correlation with elastic net penalty. *NeuroImage*, 59(4):3852–3861.

[38] Sagar, K., Banerjee, S., Datta, J., and Bhadra, A. (2024). Precision matrix estimation under the horseshoe-like prior–penalty dual. *Electronic Journal of Statistics*, 18(1):1–46.

[39] Städler, N. and Bühlmann, P. (2012). Missing values: sparse inverse covariance estimation and an extension to sparse regression. *Statistics and Computing*, 22(1):219–235.

- [40] Van de Geer, S., Bühlmann, P., Ritov, Y., Dezeure, R., et al. (2014). On asymptotically optimal confidence regions and tests for high-dimensional models. *The Annals of Statistics*, 42(3):1166–1202.
- [41] Wang, H. (2012). Bayesian graphical lasso models and efficient posterior computation. *Bayesian Analysis*, 7(4):867–886.
- [42] Zhang, R., Yao, Y., and Ghosh, M. (2022). Contraction of a quasi-bayesian model with shrinkage priors in precision matrix estimation. *Journal of Statistical Planning and Inference*, 221:154–171.

Supplementary Material for

“Censored Graphical Horseshoe: Bayesian sparse precision matrix estimation with censored and missing data”

The Tien Mai, Sayantan Banerjee

A Additional simulations results

We now provide some trace and ACF plots as well as effective sample size of the Gibbs sampler to visualize the behaviour of our algorithm.

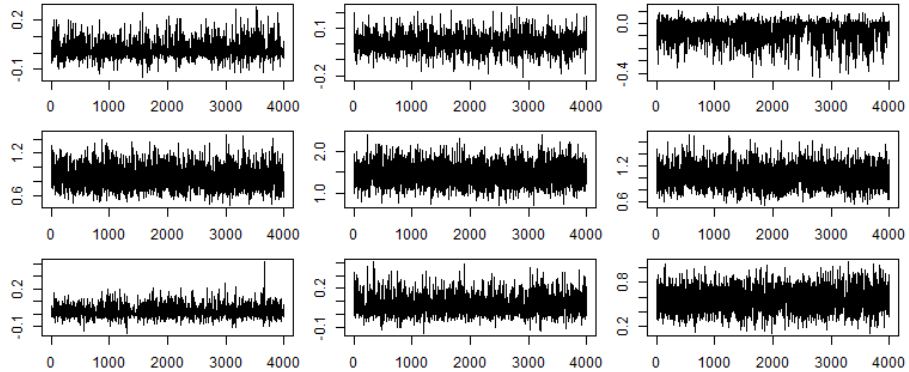


Figure 2: Trace plots from the Gibbs sampler for selected parameter entries. Top row: three randomly chosen entries with true value 0. Middle row: three randomly chosen entries with true value 1. Bottom row: three randomly chosen entries with true value 0.3. The true precision matrix is in Setting I with $p = 10, n = 100$. 10% of data being missing.

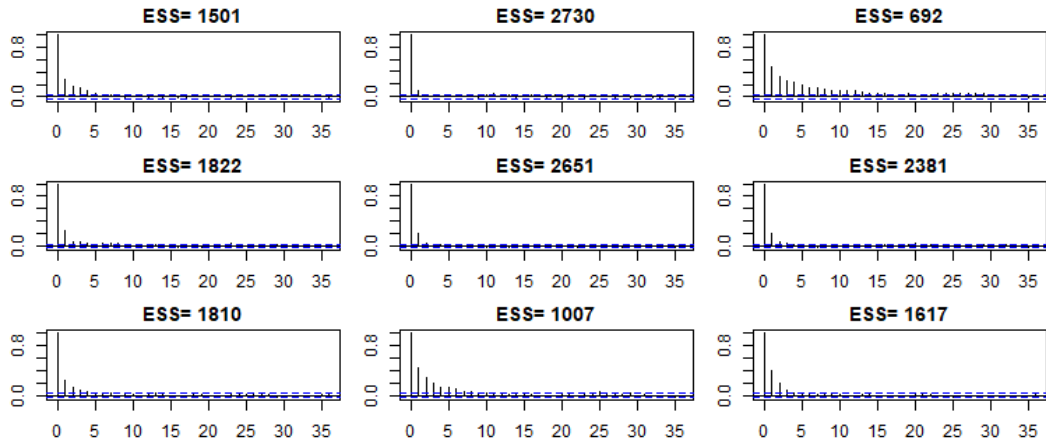


Figure 3: ACF plots from the Gibbs sampler for some random entries as in Figure 4. Top row (3 plots): 3 random entries with true value 0. Middle row (3 plots): 3 random entries with true value 1. Bottom row (3 plots): 3 random entries with true value 0.3. The ESS (effective sample size) are also given. 10% of data being missing.

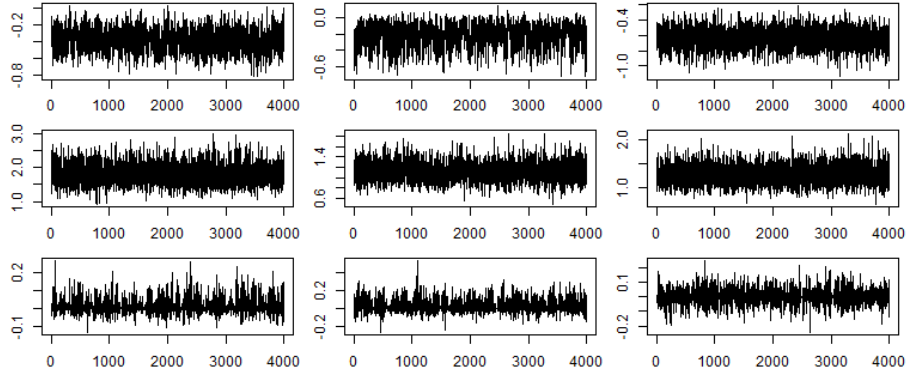


Figure 4: Trace plots from the Gibbs sampler for selected parameter entries. Top row: three randomly chosen entries with true value -0.5 . Middle row: three randomly chosen entries with true value 1 . Bottom row: three randomly chosen entries with true value 0 . The true precision matrix is in Setting II with $p = 10, n = 100$. 10% of data being missing.

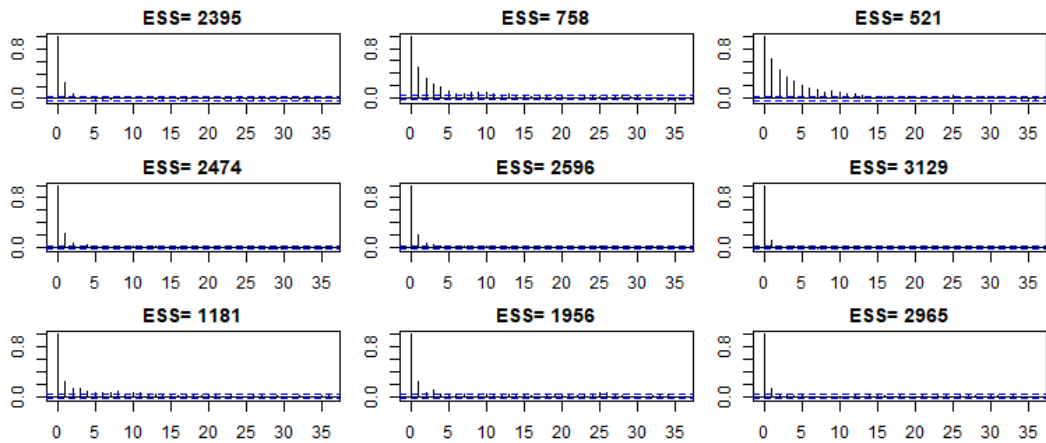


Figure 5: ACF plots from the Gibbs sampler for some random entries as in Figure 4. Top row: three randomly chosen entries with true value -0.5 . Middle row: three randomly chosen entries with true value 1 . Bottom row: three randomly chosen entries with true value 0 . The true precision matrix is in Setting II with $p = 10, n = 100$. The ESS (effective sample size) are also given. 10% of data being missing.

B Proofs

B.1 Main proof

In the proofs, K represents a positive universal constant. Its value may vary from line to line, but we use it to simplify the presentation without specifying a new constant each time.

Proof of Theorem 1. From Lemma 2, we have that $\mathcal{K}(P_{\Omega_0}, P_{\Omega}) \leq K \|\Omega - \Omega_0\|_F^2$. Define $\rho_n \propto \mathbf{1}_{\|\Omega - \Omega_0\|_2 < \delta} \Pi_{HS}$, where $\delta = [s \log(p/s)/n]^{1/2}$. We have,

$$\int \mathcal{K}(P_{\omega_0}, P_{\omega}) \rho_n(d\omega) \leq K \delta^2 = K \frac{s \log(p/s)}{n}.$$

From Lemma 1, we have,

$$\frac{1}{n} \mathcal{K}(\rho_n, \pi) \leq K \frac{s \log(p(p-1)/s)}{n} \lesssim K \frac{s \log(p)}{n}.$$

Therefore, we can apply Theorem 3 to have, for any $\alpha \in (0, 1)$,

$$\mathbb{E} \left[\int \mathcal{D}_{\alpha}(P_{\Omega}, P_{\Omega_0}) \pi_{n,\alpha}(d\Omega) \right] \leq \frac{1+\alpha}{1-\alpha} \varepsilon_n,$$

with $\varepsilon_n = Kn^{-1}s \log p$, for some universal constant $K > 0$ not depending on n, p, s . \square

Proof of Theorem 2. From Lemma 3, we have that $\mathcal{K}(P_{\Omega_0}, P_{\Omega}) \leq K \|\Omega - \Omega_0\|_F^2$. The rest of the proof is identical as above. \square

B.2 Auxiliary results

Lemma 1 (Lemma 3 in [23]). *Suppose $\omega_0 \in \mathbb{R}^d$ such that $\|\omega_0\|_0 = s^*$ and that $s^* < n < d$ and $\|\omega_0\|_{\infty} \leq C_1$. Suppose $\omega \sim \pi_{HS}$. Define $\delta_n = \{s^* \log(d/s^*)/n\}^{1/2}$. Then we have, for some constant $K > 0$, that*

$$\pi_{HS}(\|\omega - \omega_0\|_2 < \delta_n) \geq e^{-Ks^* \log(d/s^*)}.$$

and that $\mathcal{K}(\rho_n, \pi_{HS}) \leq \log \frac{1}{\pi_{HS}(\|\omega - \omega_0\|_2 < \delta_n)} \leq Ks^* \log(d/s^*)$.

We will make use of the following general result, see also [24, 28, 26, 27, 30].

Theorem 3 (Theorem 2.6 in [1]). *Assume that there exists a sequence $\varepsilon_n > 0$ and a distribution ρ_n such that*

$$\int \mathcal{K}(P_{\omega_0}, P_{\omega}) \rho_n(d\omega) \leq \varepsilon_n; \text{ and } \mathcal{K}(\rho_n, \pi) \leq n\varepsilon_n.$$

Then, for any $\alpha \in (0, 1)$,

$$\mathbb{E} \left[\int \mathcal{D}_{\alpha}(P_{\omega}, P_{\omega_0}) \pi_{n,\alpha}(d\omega) \right] \leq \frac{1+\alpha}{1-\alpha} \varepsilon_n.$$

B.2.1 Lemma for censored data

From (2), in the case of censored data, the observed-data log-likelihood of \tilde{y} is as

$$\ell(\Omega; \tilde{y}) = \frac{1}{2} \log \det(\Omega_{\mathcal{O}\mathcal{O}}) - \frac{1}{2} \tilde{y}_{\mathcal{O}}^\top \Omega_{\mathcal{O}\mathcal{O}} \tilde{y}_{\mathcal{O}} + \log \Phi_{|\mathcal{C}|}(cc; \mu_{\mathcal{C}|\mathcal{O}}(\tilde{y}_{\mathcal{O}}), \Sigma_{\mathcal{C}|\mathcal{O}}),$$

where $\mu_{\mathcal{C}|\mathcal{O}}(\tilde{y}_{\mathcal{O}}) = \Sigma_{\mathcal{C}\mathcal{O}} \Sigma_{\mathcal{O}\mathcal{O}}^{-1} \tilde{y}_{\mathcal{O}}$ and $\Sigma_{\mathcal{C}|\mathcal{O}} = \Sigma_{cc} - \Sigma_{\mathcal{C}\mathcal{O}} \Sigma_{\mathcal{O}\mathcal{O}}^{-1} \Sigma_{\mathcal{O}c}$.

Lemma 2. *Under Assumptions 1 and 3, for the censored Gaussian model and log-likelihood $\ell(\Omega; \tilde{Y})$, there exists a constant $K > 0$ depending only on m, M , and c , such that, for all $\Omega \in \mathcal{S}$,*

$$\mathbb{E}_{\Omega_0} [\ell(\Omega_0; \tilde{Y}) - \ell(\Omega; \tilde{Y})] \leq K \|\Omega - \Omega_0\|_F^2.$$

Proof of Lemma 2. *Step 1: Taylor Expansion of the Expected Log-Likelihood.* Let $L(\Omega) := \mathbb{E}_{\Omega_0} [\ell(\Omega; \tilde{Y})]$ denote the expected log-likelihood under the true precision matrix Ω_0 . Since the log-likelihood function $\ell(\Omega; \tilde{Y})$ is twice continuously differentiable with respect to Ω on the spectral band \mathcal{S} , we apply a second-order Taylor expansion of $L(\Omega)$ around Ω_0 .

Using the Lagrange form of the remainder, there exists some $\Omega^* = \Omega_0 + t(\Omega - \Omega_0)$ with $t \in (0, 1)$ such that:

$$L(\Omega) - L(\Omega_0) = \langle \Omega - \Omega_0, \nabla L(\Omega_0) \rangle + \frac{1}{2} \langle \Omega - \Omega_0, \nabla^2 L(\Omega^*)[\Omega - \Omega_0] \rangle,$$

where $\langle A, B \rangle = \text{tr}(A^\top B)$ denotes the Frobenius inner product.

Step 2: The First-Order Term Vanishes. The gradient of the expected log-likelihood, $\nabla L(\Omega)$, is given by $\mathbb{E}_{\Omega_0} [\nabla \ell(\Omega; \tilde{Y})]$. A fundamental property of maximum likelihood estimation is that the expected score at the true parameter is zero. Thus:

$$\nabla L(\Omega_0) = \mathbb{E}_{\Omega_0} [\nabla \ell(\Omega_0; \tilde{Y})] = 0.$$

Substituting this into the expansion yields:

$$L(\Omega) - L(\Omega_0) = \frac{1}{2} \langle \Omega - \Omega_0, \nabla^2 L(\Omega^*)[\Omega - \Omega_0] \rangle.$$

Rearranging to match the quantity of interest:

$$\mathbb{E}_{\Omega_0} [\ell(\Omega_0; \tilde{Y}) - \ell(\Omega; \tilde{Y})] = L(\Omega_0) - L(\Omega) = -\frac{1}{2} \langle \Omega - \Omega_0, \nabla^2 L(\Omega^*)[\Omega - \Omega_0] \rangle.$$

Step 3: Uniform Bound on the Hessian. Since \mathcal{S} is convex, the intermediate matrix Ω^* lies within \mathcal{S} . By Assumption 3, the Hessian of the expected log-likelihood is uniformly bounded on \mathcal{S} . Specifically, for any matrix Δ , the quadratic form satisfies:

$$|\langle \Delta, \nabla^2 L(\Omega^*)[\Delta] \rangle| \leq K_1 \|\Delta\|_F^2,$$

for some constant $K_1 > 0$ depending on m, M , and c .

Since the expected log-likelihood is concave, the term $\langle \Omega - \Omega_0, \nabla^2 L(\Omega^*)[\Omega - \Omega_0] \rangle$ is non-positive. Therefore:

$$-\frac{1}{2} \langle \Omega - \Omega_0, \nabla^2 L(\Omega^*)[\Omega - \Omega_0] \rangle \leq \frac{1}{2} |\langle \Omega - \Omega_0, \nabla^2 L(\Omega^*)[\Omega - \Omega_0] \rangle| \leq \frac{1}{2} K_1 \|\Omega - \Omega_0\|_F^2.$$

Setting $K = \frac{1}{2} K_1$, we obtain the desired result:

$$\mathbb{E}_{\Omega_0} [\ell(\Omega_0; \tilde{Y}) - \ell(\Omega; \tilde{Y})] \leq K \|\Omega - \Omega_0\|_F^2.$$

The constant $K > 0$ depends on m, M , and the censoring thresholds c . The proof is completed. \square

B.2.2 Lemma for missing data

We assume that the (possibly random) pattern $(\mathcal{O}_i)_{i=1}^n$ is arbitrary but independent of the unobserved values (MAR). From (6), for the case of missing data, we have the log-likelihood as

$$\ell_i(\Omega; \tilde{Y}_i) = -\frac{1}{2} \log \det(\Sigma_{\mathcal{O}_i}) - \frac{1}{2} \tilde{Y}_i^\top \Sigma_{\mathcal{O}_i}^{-1} \tilde{Y}_i.$$

Lemma 3. *Under Assumption 1, there exists a finite constant $K > 0$, depending only on m and M , such that,*

$$E_{\Omega_0} [\ell(\Omega_0; \tilde{Y}) - \ell(\Omega; \tilde{Y})] \leq K \|\Omega - \Omega_0\|_F^2.$$

Proof of Lemma 3. We prove the statement step by step and track constants.

Step 1. Fix a row i and its observed index set $O := \mathcal{O}_i$. Let $A := \Sigma_{0,O}$ and $B := \Sigma_O$ denote the corresponding principal submatrices of Σ_0 and Σ . Conditional on the pattern, $\tilde{Y}_i \sim \mathcal{N}_d(0, A)$ under the true model ($d := |O|$). The expected contribution of row i equals the KL divergence between these two centered Gaussians:

$$\delta_i := \mathbb{E}_{\Omega_0} [\ell_i(\Omega_0; \tilde{Y}_i) - \ell_i(\Omega; \tilde{Y}_i)] = \mathcal{K}(\mathcal{N}(0, A) \parallel \mathcal{N}(0, B)).$$

The standard closed form gives

$$\delta_i = \frac{1}{2} \left\{ \text{tr}(B^{-1}A) - d + \log \frac{\det B}{\det A} \right\}.$$

Step 2. Set $E := A^{-1/2}BA^{-1/2}$ (so $E \succ 0$). Then

$$\delta_i = \frac{1}{2} \left\{ \text{tr}(E^{-1}) - d + \log \det E \right\} =: \frac{1}{2} \phi(E).$$

Note $\phi(I) = 0$ and $\nabla \phi(I) = 0$ (first-order term cancels). On the spectral bounds from Assumption 3, we have

$$\lambda_{\min}(A) \geq \lambda_{\min}(\Sigma_0) \geq 1/M, \quad \lambda_{\max}(A) \leq \lambda_{\max}(\Sigma_0) \leq 1/m,$$

and similarly for B . Hence the eigenvalues of E lie in the compact interval $[m/M, M/m]$. Let \mathcal{S} denote the set of such E (with dimension at most p). The function ϕ is twice continuously differentiable on \mathcal{S} , hence its Hessian is bounded there; write

$$H_{\max} := \sup_{E \in \mathcal{S}} \|\text{Hess } \phi(E)\|_{\text{op}} < \infty.$$

By the second-order Taylor formula with integral remainder (or the mean-value form of the remainder) applied at I ,

$$\phi(E) = \frac{1}{2} \langle E - I, \text{Hess } \phi(\xi)[E - I] \rangle \leq \frac{1}{2} H_{\max} \|E - I\|_F^2$$

for some ξ on the segment between I and E . Consequently

$$\delta_i = \frac{1}{2} \phi(E) \leq \frac{H_{\max}}{4} \|E - I\|_F^2.$$

Step 3. Observe that $E - I = A^{-1/2}(B - A)A^{-1/2}$. Hence

$$\|E - I\|_F \leq \|A^{-1/2}\|_2^2 \|B - A\|_F = \frac{1}{\lambda_{\min}(A)} \|B - A\|_F.$$

Because $\lambda_{\min}(A) \geq 1/M$ we get $\|E - I\|_F \leq M \|B - A\|_F$. Therefore

$$\delta_i \leq \frac{H_{\max}}{4} M^2 \|B - A\|_F^2.$$

Step 4. We use the exact identity

$$\Sigma - \Sigma_0 = \Omega^{-1} - \Omega_0^{-1} = \Omega^{-1}(\Omega_0 - \Omega)\Omega_0^{-1}.$$

Therefore with the operator-norm bounds $\|\Omega^{-1}\|_2, \|\Omega_0^{-1}\|_2 \leq 1/m$,

$$\|\Delta\|_F \leq \|\Omega^{-1}\|_2 \|\Omega_0^{-1}\|_2 \|\Omega - \Omega_0\|_F \leq \frac{1}{m^2} \|\Omega - \Omega_0\|_F.$$

Combining with the previous step yields

$$\Delta(\Omega) \leq \frac{H_{\max}}{4} \frac{M^2}{m^4} \|\Omega - \Omega_0\|_F^2.$$

This proves the claimed upper bound. \square